Journal of Power Sources 430 (2019) 150–156

Contents lists available at ScienceDirect

Journal of Power Sources

journal homepage: www.elsevier.com/locate/jpowsour

Rate capability of carbon-free lithium titanium oxide electrodes related to formation of electronic conduction paths observed by color change

Kingo Ariyoshi *, Takaya Ino, Yusuke Yamada **

Department of Applied Chemistry and Bioengineering, Graduate School of Engineering, Osaka City University, 3-3-138 Sugimoto, Sumiyoshi-ku, Osaka, 558-8585, Japan

ARTICLE INFO

Keywords:
Lithium-ion battery
Lithium titanium oxide
Rate capability
Electronic conductivity

ABSTRACT

Lithium titanium oxide prepared by the hydrogen reduction synthesis of $Li[Li_{1/3}Ti_{5/3}]O_4$ (LTO) exhibits electronic conductivity. The product demonstrated a superior rate capability than pristine LTO upon the examination of a pellet electrode in the absence of conductive additives. The rate capability of the pristine LTO pellet electrode is poor during the oxidation reaction due to low electronic conductivity of the electrode originated from insufficiently developed electronic conduction paths. In contrast, the rate capability during the reduction reaction is improved due to the formation of electronic conduction paths resulting from transformation to the electronic conductor LTO during the reduction process. Visual inspection indicated that the formation and loss of electronic conduction paths in the electrode are key to determining the rate capability of the LTO pellet electrode in the absence of a conductive additive. Our results confirmed that this LTO exhibiting an electronic conductivity maintains an electronic conduction path in the pellet electrode in the absence of a conductive additive during the redox reaction, thereby resulting in an improved rate capability in both the oxidation and reduction reactions.

1. Introduction

Among the various metal oxides for negative electrodes in lithium-ion batteries reported so far [1–4], the zero-strain lithium insertion material derived from lithium titanium oxide ($Li[Li_{1/3}Ti_{5/3}]O_4$; LTO) is one of the attractive materials [5–7], because it has no cycle life limitation, no risk of Li metal deposition, and a low reactivity with an electrolyte due to the relatively noble electrode potential of ~1.55 V versus the Li metal electrode. Due to such advantageous properties, LTO has been widely used as a negative electrode material in lithium-ion batteries containing positive electrodes [8–13], such as $LiFePO_4$ [8], $LiCo_{1/3}Ni_{1/3}Mn_{1/3}O_2$ [10], and $Li[Ni_{1/2}Mn_{3/2}]O_4$ [12], in addition to being applied in lithium-ion asymmetric capacitors containing graphitized carbon [14,15]. During the last decade, the rate capability of LTO, which is a crucial factor to obtain high power lithium-ion battery, has been improved by a number of methods [16–26] including metal doping [17,18], nano-sizing [19–22], and surface coating [23–26].

As pristine LTO is an inherent insulator, a carbon additive is required to construct electronic conduction paths in an LTO electrode. The surface modification of LTO by a carbon or metal coating thereby enhances the electronic conductivity of LTO particles, resulting in the construction of electronic conduction paths in the LTO electrodes. Recently, surface modification through reduction synthesis has been carried out to form metal ions with low oxidation states, which enhance the electronic conductivity of LTO [27–30]. For example, LTO prepared under hydrogen to form oxygen-deficient LTO, i.e., $Li_{4/3}Ti_{5/3}O_{4-\delta}$, which is either blue or dark blue, exhibits an improved electronic conductivity [27–29]. In addition, Mo doping enhances the electronic conductivity of LTO [30], because the two d-electrons of a Mo^{4+} ion contribute to the electronic conduction. Both of these LTOs showed superior rate capabilities to the pristine material.

However, in these studies the electrodes always contained conductive carbon (~10 wt%) to examine the rate capability of the LTOs exhibiting electronic conductivity, although LTOs with high or medium electronic conductivities require no conductive additive to be used as an electrode. This is of importance, as reducing the quantities of conductive additives is beneficial in the design of high energy density lithium-ion batteries. Furthermore, an electrode material exhibiting electronic conductivity is suitable for all solid-state batteries, because electronic and ionic conduction paths are easily constructed within the electrode by mixing active materials and a Li-ion conductor without conductive carbon.

* Corresponding author.
** Corresponding author.
E-mail addresses: ariyoshi@osaka-cu.ac.jp (K. Ariyoshi), ymd@a-chem.eng.osaka-cu.ac.jp (Y. Yamada).

https://doi.org/10.1016/j.jpowsour.2019.05.023
Received 31 January 2019; Received in revised form 25 April 2019; Accepted 6 May 2019
Available online 16 May 2019

We herein report the rate capability of LTO examined using a pellet-type electrode without conductive additives and polymer binders. The LTO was prepared by hydrogen reduction synthetic route to achieve electronic conductivity. In addition, differences in the rate capabilities of two kinds of LTO (i.e., an electronic conductor and an insulator) are discussed with emphasis on the electronic conduction paths within the electrodes.

2. Materials and methods

2.1. Synthesis and characterization of the electronic conductive LTO

Lithium titanium oxide, $Li[Li_{1/3}Ti_{5/3}]O_4$, (LTO; LT 855-17C, Ishihara Sangyo) powder was used as the pristine sample. Prior to use, the electrochemical properties of LTO were confirmed using a conventional electrode containing a conductive additive and a binder. The electrodes were examined in lithium cells with a lithium metal electrode using charge-discharge tests at a constant current density (0.5 mA cm^{-2}). The LTO used in this study exhibited a reversible capacity >150 mAh g^{-1}, a voltage difference between charge and discharge <100 mV, and no noticeable capacity fading during cycling.

For the hydrogen reduction process, the LTO powder was placed in an alumina boat and dehydrated at 200 °C for 1 h under a flow of nitrogen, then heated at the desired temperature for 3 h under a hydrogen atmosphere. After this time, the temperature was reduced to ~200 °C, and the sample was subjected to a flow of nitrogen gas for ~10 min prior to removal of the sample. The LTO samples prepared by this approach were characterized by X-ray diffraction (XRD), scanning electron microscopy (SEM), thermogravimetric (TG) analysis, and electrochemical measurements.

As mentioned above, the crystal structure of the prepared LTO was determined by powder XRD measurements using an X-ray diffractometer (XRD-6100, Shimadzu, Co., Japan) equipped with a graphite monochromator. As the X-ray source, an iron tube (wavelength: $\lambda = 1.93579$ Å) was used. The tube voltage and current were 40 kV and 15 mA, respectively. The measurement range was 10°–100° (2θ) and the scanning rate was 0.5° min^{-1}. The lattice constant was calculated by the least squares method using 8 diffraction lines. Particle morphology of LTOs were observed by a SEM (VE-7800, Keyence Co., Japan). TG analysis (TGA-50, Shimadzu, Co., Japan) was carried out by placing the sample (~20 mg) on a platinum dish and heating to 1000 °C prior to subsequent cooling to 200 °C at a rate of 10 °C min^{-1} under a flow of dry air (flow rate = 20 mL min^{-1}).

Pellet electrodes free from conductive additives and binders were employed. To form the pellet electrode, the LTO electrode was pressed under a pressure of 0.6 GPa for 10 min to give a pellet with an electrode area of 1.3 cm^2. The electrode weights were ~100 mg for the pristine LTO, and ~50 mg for the LTO prepared by the hydrogen reduction route. Details regarding the electrochemical cell and the charge-discharge instruments can be found in the literature [7]. The electrolyte employed herein was 1 M $LiPF_6$ containing an ethylene carbonate (EC) and dimethyl carbonate (DMC) solution (EC:DMC = 3:7) (Kishida Chemical Co., Ltd., Japan). Two sheets of microporous membranes (Celgard 2500 and Celgard 2320) were used as the separator to avoid an internal short circuit due to the dendrite formation of lithium metal.

2.2. Color changes of a pristine LTO pellet electrode during the initial cycle

A visualization cell was employed to observe the color change of the pristine LTO electrode during charging and discharging. In the visualization cell, the stainless steel container was replaced with a clear acrylic polymer plate. A strip of copper foil was used for a current collector. A galvanostat (HA-151, Hokuto Denko Co., Japan) was used for the charge-discharge tests, during which the LTO electrode was reduced to 1 V at a constant current (0.5 mA) then oxidized at 1 mA until reaching 3 V, and subsequently oxidized at a constant voltage of 3 V.

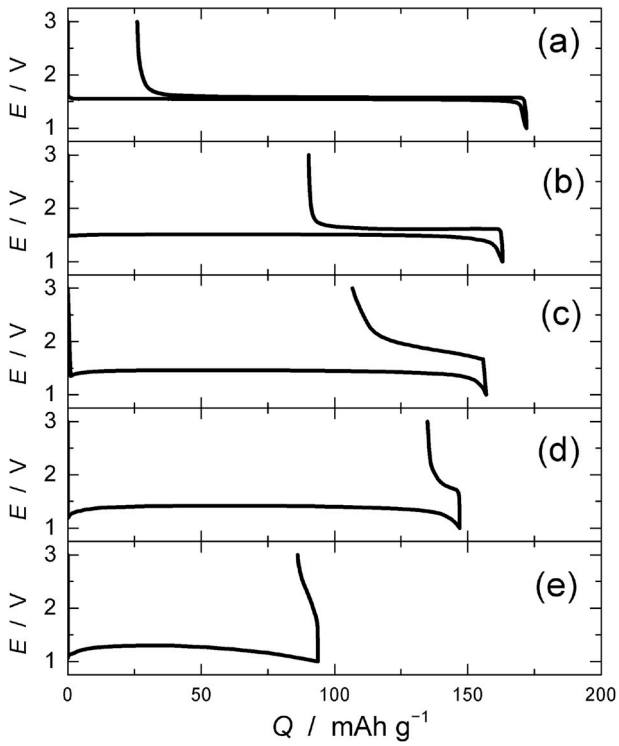

Fig. 1. Initial charge-discharge curves for the Li/LTO cells operated in the voltage range of 1–3 V at constant currents of (a) 0.1 mA, (b) 1.2 mA, (c) 3.0 mA, (d) 5.0 mA, and (e) 7.0 mA. The weights of the pellet LTO electrodes were (a) 44.4 mg, (b) 45.9 mg, (c) 45.9 mg, (d) 46.9 mg, and (e) 44.5 mg. The electrode area was 1.3 cm^2.

3. Results and discussion

3.1. Rate capability tests for the Li/LTO cell

Charge-discharge tests were carried out for the LTO pellet electrode in the absence of conductive additives and binders using lithium cells with a lithium metal negative electrode (Fig. 1). In the rate capability test, the cell was cycled at a constant current from 0.01 to 7.0 mA (1.3 cm^2 electrode area). The charge-discharge curves shown in Fig. 1 correspond to the initial cycle due to the poor reversibility exhibited by the LTO pellet electrodes. As the LTO is usually employed as a negative electrode in lithium-ion batteries, the charge and discharge operation is opposite for a lithium cell. To avoid complication of the terminology, the terms “reduction” and “oxidation” are used instead of “charge” and “discharge,” where the charge reaction of an LTO negative electrode in a lithium-ion battery corresponds to a reduction (lithium insertion) reaction, and the discharge reaction corresponds to an oxidation (lithium extraction) reaction. Upon increasing the applied current, the initially flat reduction curve became slightly parabolic in shape, while the flat oxidation curve became sloped. In addition, the reduction capacity decreased gradually upon increasing the applied current. At a current < 5 mA, the LTO pellet electrode delivered >155 mAh g^{-1} of reduction capacity, corresponding to ~90% of the theoretical capacity of LTO (*i.e.,* 175 mAh g^{-1}). At 7 mA, the reduction capacity decreased to 94 mAh g^{-1}. In contrast, the oxidation capacity decreased significantly from 146 to 50 mAh g^{-1} upon increasing the applied current from 0.1 to 3.0 mA. No noticeable oxidation capacity was observed at 7 mA.

The oxidation and reduction capacities of the LTO pellet electrode as a function of current are shown in Fig. 2. As indicated, the rate capabilities of the LTO electrode differed between the oxidation and

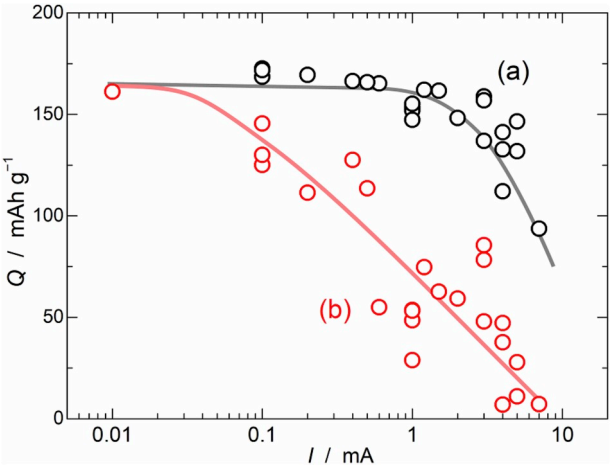

Fig. 2. The initial (a) reduction and (b) oxidation capacities of the Li/LTO cells operated in the voltage range of 1–3 V at a constant current.

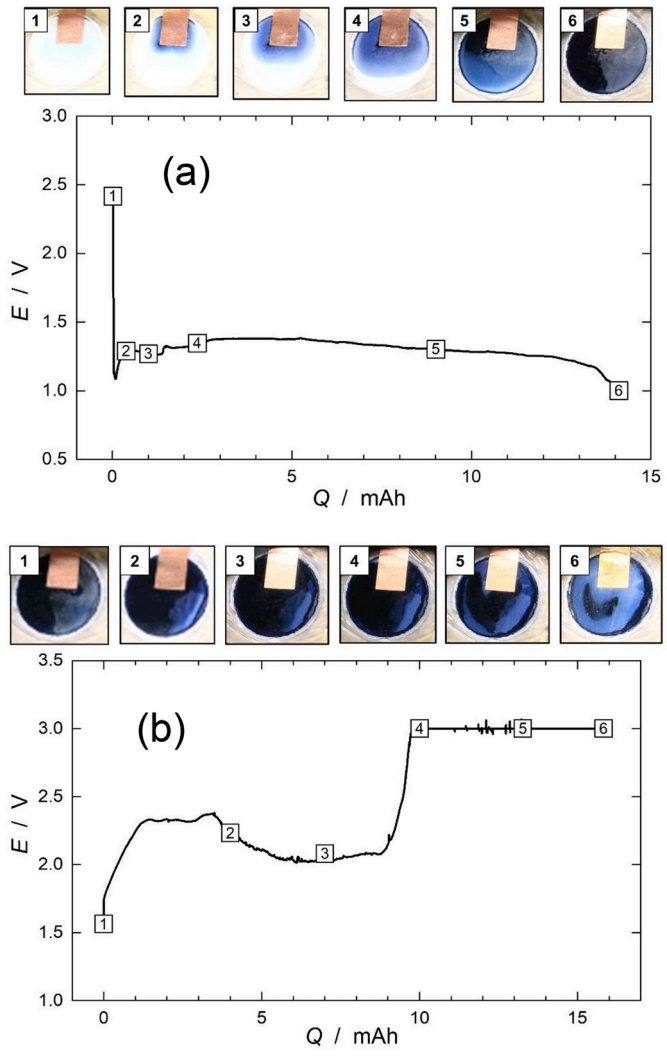

Fig. 3. (a) Reduction and (b) oxidation curves and photographic images of the color changes of an LTO electrode during the initial reduction and oxidation. (For interpretation of the references to color in this figure legend, the reader is referred to the Web version of this article.)

reduction reactions, *i.e.*, the reduction capacity was larger than

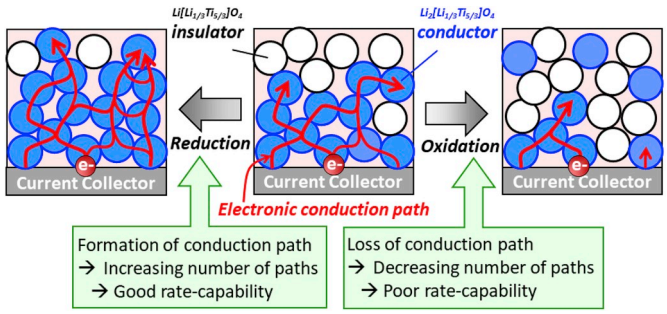

Fig. 4. Schematic illustration of color change of LTO pellet-electrode in the absence of a conductive additive. (For interpretation of the references to color in this figure legend, the reader is referred to the Web version of this article.)

oxidation capacity at each current examined. In addition, the LTO pellet electrode delivered oxidation and reduction capacities close to the theoretical values at low currents (0.1 mA), although the reduction capacity decreased sharply beyond ~1 mA, while the oxidation capacity gradually decreased beyond 0.1 mA. At higher current values (3 mA), the reduction capacity decreased slightly to 91% of that obtained at a low current density, whereas the oxidation capacity decreased significantly to 34% of the previous value. Although data variations were observed, in general, the oxidation capacity decreased in proportion to the logarithmic value of the current. These results indicate that the rate capability of the LTO pellet electrode in the absence of any conductive additive differs between the reduction and oxidation reactions. More specifically, the electronic conductivity of LTO changes from an electronic insulator to a conductor during reduction and vice versa upon oxidation. This may account for differences in the rate capability during the reduction and oxidation reactions for the LTO pellet electrode, as the absence of a conductive additive induces a poor electronic conduction path.

3.2. Color change accompanying the reaction of the LTO electrode

To elucidate the differences in the rate capability during the reduction and oxidation reactions for the LTO pellet electrode with emphasis on the formation and loss of electronic conduction paths, changes in the color of the electrode were monitored using a visualization cell, where the LTO pellet electrode was reduced at constant current of 1 mA. As shown in Fig. 3a, the color of the LTO changed from white to light blue around the current collector at the beginning of the reduction reaction. This blue region gradually expanded from the current collector side to the edge. After reduction for 2 mAh, the electrode exhibited a blue color prior to becoming dark blue or black. After the reduction reaction had proceeded to a capacity of 14.1 mAh, which is approximately equal to the theoretical capacity, the color of the LTO electrode also became dark blue. This dark blue region indicated the presence of an electronic conductor, and so an electronic conduction path was clearly formed in this case in the absence of a conductive additive.

The subsequent oxidation reaction was performed by applying a constant current of 1 mA and then a constant voltage of 3 V after the cell voltage reached 3 V. As shown in Fig. 3b, the change in color of the LTO electrode was not clearly observed in the early stages of the oxidation reaction. However, upon completion of the oxidation process, the electrode had adopted a slight light blue color. Interestingly, allowing oxidation to continue for 1 week resulted in the formation of a white electrode. These different trends in color change observed for the LTO pellet electrode during reduction and oxidation indicate that the formation and loss of electronic conduction paths in the electrode proceeded in a different manner during the reduction and oxidation reactions. This therefore accounts for the difference in the rate capability of the pristine LTO electrode (Fig. 4). Reduction of the LTO electrode results in increase of electronic conductivity, which allows to form

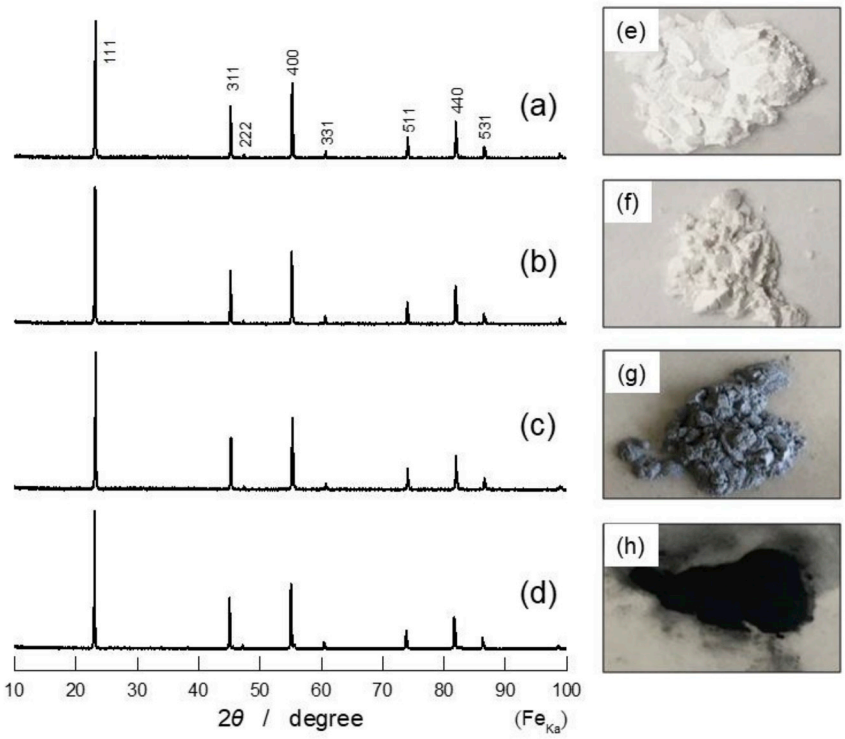

Fig. 5. XRD patterns and photographic images of (a, e) LTO and the reduced LTO prepared by heating at (b, f) 400 °C, (c, g) 700 °C, and (d, h) 900 °C for 3 h under a hydrogen atmosphere. The cubic lattice constants obtained by the least squares method using 8 diffraction lines were (a) a = 8.357 Å, (b) a = 8.360 Å, (c) a = 8.353 Å, and (d) a = 8.377 Å.

electronic conduction paths in the electrode even without conductive additive. The LTO becomes an insulator from an electronic conductor during oxidation, resulting in the loss of electron conduction paths. Electronic conduction paths diminish more rapidly, and thus, the number of electronically isolated LTO particles increases at higher current density. Consequently, the rate capability of the LTO during the oxidation reaction is poor in contrast to that during the reduction reaction.

3.3. Synthesis of the electronic conducting LTO by the hydrogen reduction route

The poor rate capability during the oxidation reaction of the LTO pellet electrode is thought to account for the poor electronic conduction path in the electrode. In other words, the LTO pellet electrode is expected to show a good rate capability in the absence of a conductive additive if the LTO exhibits electronic conductivity. To prepare such an LTO material showing electronic conductivity, LTO was heated under a stream of hydrogen to form Ti^{3+} through the reduction of Ti^{4+}. As shown in Fig. 5, the XRD patterns of the prepared LTO show little variation, indicating that the spinel structure is maintained during the reduction process. In addition, the lattice constant calculated by the least squares method from the eight diffraction lines indexed by Millar indices is essentially equal (within the range of experimental error), *i.e.*, $a = 8.36$ Å, with the exception of the LTO reduced at 900 °C, where $a = 8.377$ Å. This difference is due to the formation of trivalent Ti ions with a larger ionic radius of $r = 0.670$ Å compared with that of the tetravalent Ti ions of $r = 0.605$ Å. In addition, LTOs form a solid-solution of $Li[Li_xTi_{2-x}]O_4$ ($0 \le x \le 1/3$) between $Li[Li_{1/3}Ti_{5/3}]O_4$ and $LiTi_2O_4$ and exhibit the same spinel structure [31,32]. These observations therefore suggest that LTO prepared by the hydrogen reduction route produces a solid-solution in which a small amount of Ti^{3+} exists in the LTO:

$$2Li_4Ti_5O_{12} + 5/2nH_2 \rightarrow Li_{8-3n}Ti_{10}O_{24-4n} + 3/2nLi_2O + 5/2nH_2O$$

In the extreme case, the above equation can be simplified as follows,

$$2Li_4Ti_5O_{12} + 5/2H_2 \rightarrow 5LiTi_2O_4 + 3/2Li_2O + 5/2H_2O$$

The LTO powder produced by the hydrogen reduction route at 700 °C exhibited a partial change in color from white to blue (Fig. 5 e-h). In contrast, in the case of the LTO reduced at 900 °C, a dark blue or black powder was obtained. For the pristine LTO, secondary particles with spherical shape ca. 10 μm in diameter are agglomerate of sub-micrometer primary particles. The particle morphology of LTO did not change during the hydrogen reduction processes (Fig. S1). These color changes indicate that the electronic conductivity of LTO was enhanced upon reduction at temperatures >700 °C due to the reduction of Ti ions from the tetravalent to the trivalent state. More specifically, at higher reduction temperatures, the fraction of Ti^{3+} increases, leading to a darker color. To confirm the formation of Ti^{3+} ions in the LTO reduced at 900 °C, TG analysis was performed under air. Upon heating, the LTO weight increased beyond ~400 °C, and then decreased at ~700 °C. Upon cooling, the sample weight remained constant, and the sample weight after the TG measurements was +1.5 wt% based on the initial weight. If this weight gain is attributed to oxygen uptake associated with the oxidation of Ti^{3+} in LTO, the Ti^{3+} fraction can be calculated to be ~15%. Hence, the formula of the LTO reduced at 900 °C can be derived as $Li[Li_{0.23}Ti^{3+}_{0.3}Ti^{4+}_{1.47}]O_4$. Indeed, the observed lattice constant of $a = 8.377$ Å corresponds with that reported previously for this chemical composition [32]. The reduced LTOs are expected to have medium or high electronic conductivity, because Mg-substituted LTO containing Ti^{3+}, thus, regarded as a reduced-LTO analog [33], has been reported to show extremely high electronic conductivity compared with pristine LTO.

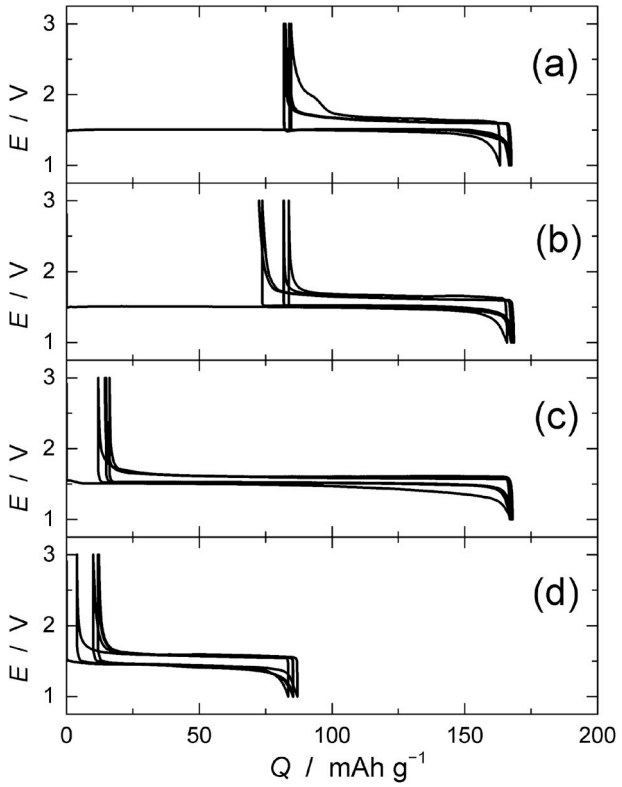

Fig. 6. Charge-discharge curves of (a) a Li/pristine LTO cell, and (b–d) Li/reduced LTO cells operated at 1.0 mA in the voltage range of 1–3 V. The initial 5 cycles were shown. Reduced LTO was prepared by heating at (b) 400 °C, (c) 700 °C, and (d) 900 °C for 3 h under a hydrogen atmosphere. The weights of the electrodes employed were (a) 96.8 mg, (b) 98.8 mg, (c) 101.1 mg, and (d) 84.6 mg, respectively. The electrode area was 1.3 cm^2.

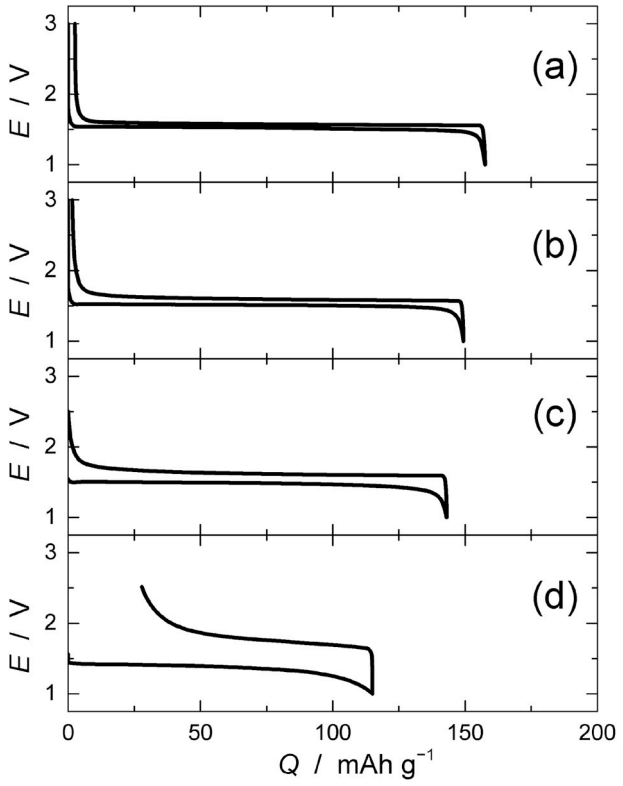

Fig. 7. Rate capability tests of the Li/blue-LTO cells operated in the voltage range of 1–3 V at constant currents of (a) 0.5 mA, (b) 1.0 mA, (c) 2.0 mA, and (d) 5.0 mA. The blue-LTO powder was prepared by heating LTO at 700 °C for 3 h under a hydrogen atmosphere. The weights of the blue-LTO electrodes were (a) 92.9 mg, (b) 92.9 mg, (c) 92.8 mg, and (d) 92.8 mg. The electrode area was 1.3 cm^2.

3.4. Electrochemical properties of the blue-LTO electrode in the absence of a conductive additive

To investigate the electrochemical characteristics of the LTO prepared by hydrogen reduction at various temperatures, a constant current charge-discharge test was conducted in the Li/LTO cells (Fig. 6). Pellet electrodes composed of only LTO powder were used to elucidate the effects of electronic conductivity on the electrochemical properties of LTO. It was found that the reduction and oxidation capacities changed depending on the color of the LTO powder. More specifically, the white-LTO produced below 700 °C gave a reduction capacity of 160 mAh g^{-1} in the initial cycle and a reversible capacity of 80 mAh g^{-1} for subsequent cycles. In addition, the blue-LTO reduced at 700 °C exhibited a large reversible capacity with a high coulombic efficiency, while the reversible capacity of the black-LTO obtained by reduction at 900 °C was approximately half of the theoretical capacity despite its high coulombic efficiency. From these results, it is apparent that the electronic conducting LTO undergoes a reversible Li insertion/extraction reaction even in the absence of a carbon additive. This results from the construction of electronic conduction paths in the electrode during the reaction, as the blue-LTO itself exhibits electronic conductivity.

The rate capability of the blue-LTO synthesized by reduction at 700 °C, which showed the largest reversible capacity among the various LTOs, was then examined. As shown in Fig. 7, upon increasing the current to 2 mA, no significant capacity loss was observed in the Li/blue-LTO cells despite a slight increase in polarization. In addition, the oxidation capacities were equal to the reduction capacities, resulting in 100% of the coulombic efficiency being exhibited for the reaction. Upon increasing the current to 5 mA, the reduction capacity was maintained at 115 mAh g^{-1}, which corresponds to two thirds of the theoretical capacity. Although the oxidation capacity was smaller than the reduction capacity, more than half of the theoretical capacity was observed. Even at the high current applied to the Li/blue-LTO cells, the voltage profiles maintained a flat shape, which is characteristic of LTO when taking part in a two-phase reaction. These results therefore indicate that blue-LTO exhibits a good rate capability despite the electrodes being composed of only an active material and without the addition of a

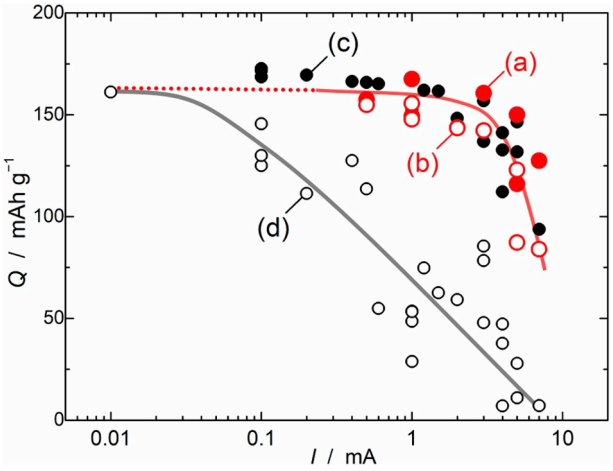

Fig. 8. The initial (a) reduction and (b) oxidation capacities of the Li/blue-LTO cells, and (c and d) those of the Li/white-LTO cells operated in the voltage range of 1–3 V. (For interpretation of the references to color in this figure legend, the reader is referred to the Web version of this article.)

conductive additive.

The oxidation and reduction capacities of the Li/blue-LTO cells are outlined in Fig. 8 and compared with those of Li/white-LTO cells. The Li/blue-LTO cells exhibited good rate capabilities in both the oxidation and reduction reactions, while the Li/white-LTO cells exhibited a poor rate capability in the oxidation reaction. In addition, the rate capability of the blue-LTO in the oxidation reaction was greatly improved by enhancing the electronic conductivity. Usually, increasing an electrode weight results in poor rate capability. The weight of blue-LTO electrode is larger than that of white-LTO electrode, however, the blue-LTO exhibits better rate capability than the white-LTO. Therefore, the weight difference of these two electrode insignificantly affects the trend of rate capability (blue > white). The capacity retention in the oxidation and reduction reactions for the Li/blue-LTO cells was similar to that in the reduction reaction for the Li/white-LTO cell. This indicates that the decrease in capacity for the rate-capability tests of blue-LTO is related to Li ion transportation within the electrode, rather than to electronic conductivity. As the blue-LTO is an electronic conductor due to the partial formation of Ti^{3+} in LTO during the hydrogen reduction process, the electronic conduction path inside the electrode is maintained in the blue-LTO electrodes during lithium insertion/extraction reactions. It is noticed that there is no crucial difference between electro-reduction and hydrogen reduction in the formation of Ti^{3+} of the LTO. Therefore, both pristine and hydrogen-reduced LTOs show the same rate capability during reduction reaction. On the other hand, during oxidation reaction, the hydrogen-reduced LTO maintains electronic conductivity, resulting in the superior rate capability in contrast to pristine LTO, because Ti^{3+} ions remained in the hydrogen-reduced LTO even at fully oxidized state.

The excellent rate capability of the blue-LTO electrode therefore originated from the formation of electronic conduction paths in the electrodes in the absence of a conductive additive.

4. Conclusions

The rate capabilities of pristine lithium titanium oxide (LTO) and LTOs prepared using the hydrogen reduction synthetic route were examined using pellet electrodes without the addition of any conductive additive or binder. Our results showed that pristine white-LTO was an inherent insulator that exhibited a poor rate capability in the oxidation reaction despite a superior rate capability in the reduction reaction. In addition, the color changes in the white-LTO pellet electrode monitored using a visualization cell indicated that the formation or loss of an electronic conduction path during the reduction or oxidation reaction, respectively, resulted in different rate capabilities for the white-LTO electrode. Furthermore, the electronic conductive blue-LTO prepared by the hydrogen reduction route exhibited a superior rate capability to the white-LTO in both the reduction and oxidation reactions due to an electronic conduction path being maintained in the blue-LTO electrodes during the reaction. These results are of importance, as no conductive additives were required to enhance the rate capability of the LTO, and this is beneficial in the design of high-energy density lithium-ion batteries and all solid-state batteries.

Acknowledgement

This work was partly supported by Advanced Low Carbon Technology Research and Development Program, Specially Promoted Research for Innovative Next Generation Batteries (ALCA Spring) from the Japan Science and Technology Agency (JST), Japan.

Appendix A. Supplementary data

Supplementary data to this article can be found online at https://doi.org/10.1016/j.jpowsour.2019.05.023.

References

[1] P. Roy, S.K. Srivastava, Nanostructured anode materials for lithium ion batteries, J. Mater. Chem. A 3 (2015) 2454–2484.
[2] Y. Zhao, X. Li, B. Yan, D. Xiong, D. Li, S. Lawes, X. Sun, Recent developments and understanding of novel mixed transition-metal oxides as anodes in lithium ion batteries, Adv. Energy Mater. 6 (2016) 1502175.
[3] X.S. Zhou, L. Yu, X.W. Lou, Formation of uniform N-doped carbon-coated SnO_2 submicroboxes with enhanced lithium storage properties, Adv. Energy Mater. 6 (2016) 1600451.
[4] W. Weng, J. Lin, Y. Du, X. Ge, X. Zhou, J. Bao, Template-free synthesis of metal oxide hollow micro-/nanospheres via Ostwald ripening for lithium-ion batteries, J. Mater. Chem. 6 (2018) 10168–10175.
[5] T. Ohzuku, A. Ueda, N. Yamamoto, Zero-strain insertion material of $Li[Li_{1/3}Ti_{5/3}]O_4$ for rechargeable lithium cells, J. Electrochem. Soc. 142 (1995) 1431–1435.
[6] S. Scharner, W. Weppner, P. Schmid-Beurmann, Evidence of two-phase formation upon lithium insertion into the $Li_{1.33}Ti_{1.67}O_4$ spinel, J. Electrochem. Soc. 146 (1999) 857–861.
[7] K. Ariyoshi, R. Yamato, T. Ohzuku, Zero-strain insertion mechanism of $Li[Li_{1/3}Ti_{5/3}]O_4$ for advanced lithium-ion (shuttlecock) batteries, Electrochim. Acta 51 (2005) 1125–1129.
[8] K. Zaghib, M. Dontigny, A. Cuerfi, P. Charest, I. Rodrigues, A. Mauger, C.M. Julien, Safe and fast-charging Li-ion battery with long shelf life for power applications, J. Power Sources 196 (2011) 3949–3954.
[9] N. Takami, K. Yoshida, Y. Harada, 12 V-class bipolar lithium-ion batteries using $Li_4Ti_5O_{12}$ anode for low-voltage system applications, J. Electrochem. Soc. 164 (2017) A6254–A6259.
[10] N. Takami, H. Inagaki, Y. Tatebayashi, H. Saruwatari, K. Honda, S. Egusa, High-power and long-life lithium-ion batteries using lithium titanium oxide anode for automotive and stationary power applications, J. Power Sources 244 (2013) 469–475.
[11] I. Belharouak, Y.-K. Sun, W. Lu, K. Amine, On the safety of the $Li_4Ti_5O_{12}/LiMn_2O_4$ lithium-ion battery system, J. Electrochem. Soc. 154 (2007) A1083–A1087.
[12] K. Ariyoshi, S. Yamamoto, T. Ohzuku, Three-volt lithium-ion battery with $Li[Ni_{1/2}Mn_{3/2}]O_4$ and the zero-strain insertion material of $Li[Li_{1/3}Ti_{5/3}]O_4$, J. Power Sources 119–121 (2003) 959–963.
[13] J. Barker, R.K. Gover, P. Burns, A.J. Bryan, A lithium-ion cell based on $Li_{4/3}Ti_{5/3}O_4$ and $LiVPO_4F$, Electrochem. Solid State Lett. 10 (2007) A130–A133.
[14] G.G. Amatucci, F. Badway, A.D. Pasquier, T. Zheng, An asymmetric hybrid nonaqueous energy storage cell, J. Electrochem. Soc. 148 (2001) A930–A939.
[15] A.D. Pasquier, I. Plitz, S. Menocal, G. Amatucci, A comparative study of Li-ion battery, supercapacitor and nonaqueous asymmetric hybrid devices for automotive applications, J. Power Sources 115 (2003) 171–178.
[16] B. Zhao, R. Ran, M. Liu, Z. Shao, A comprehensive review of $Li_4Ti_5O_{12}$-based electrodes for lithium-ion batteries: the latest advancements and future perspective, Mater. Sci. Eng. R 98 (2015) 1–71.
[17] A.D. Robertson, L. Trevino, H. Tukamoto, J.T.S. Irvine, New inorganic spinel oxides for use as negative electrode materials in future lithium-ion batteries, J. Power Sources 81–82 (1999) 352–357.
[18] P. Kubiak, A. Garcia, M. Womes, L. Aldon, J. Olivier-Fourcade, P.-E. Lippens, J.-C. Jumas, Phase transition in the spinel $Li_4Ti_5O_{12}$ induced by lithium insertion: influence of the substitutions Ti/V, Ti/Mn, Ti/Fe, J. Power Sources 119–121 (2003) 626–630.
[19] K. Amine, I. Belharouak, Z. Chen, T. Tran, H. Yumoto, N. Ota, S.-T. Myung, Y.-K. Sun, Nanostructured anode material for high-power battery system in electric vehicles, Adv. Mater. 22 (2010) 3052–3057.
[20] J. Haetge, P. Hartmann, K. Brezesinski, J. Janek, T. Brezesinski, Ordered large-pore mesoporous $Li_4Ti_5O_{12}$ spinel thin film electrodes with nanocrystalline framework for high rate rechargeable lithium batteries: relationships among charge storage, electrical conductivity, and nanoscale structure, Chem. Mater. 23 (2011) 4384–4393.
[21] A.S. Prakash, P. Manikandan, K. Ramesha, M. Sathiya, J.-M. Tarascon, A.K. Shukla, Solution-combustion synthesized nanocrystalline $Li_4Ti_5O_{12}$ as high-rate performance Li-ion battery anode, Chem. Mater. 22 (2010) 2857–2863.
[22] E. Kang, Y.S. Jung, G.-H. Kim, J. Chun, U. Wiesner, A.C. Dillon, J.K. Kim, J. Lee, Highly improved rate capability for a lithium-ion battery nano-$Li_4Ti_5O_{12}$ negative electrode via carbon-coated mesoporous uniform pores with a simple self-assembly method, Adv. Funct. Mater. 21 (2011) 4349–4357.
[23] G.-N. Zhu, H.-J. Liu, J.-H. Zhuang, C.-X. Wang, Y.-Y. Xia, Carbon-coated nano-sized $Li_4Ti_5O_{12}$ nanoporous micro-sphere as anode material for high-rate lithium-ion batteries, Energy Environ. Sci. 4 (2011) 4016–4022.
[24] N. Li, G. Zhou, F. Li, L. Wen, H.-M. Cheng, A self-standing and flexible electrode of $Li_4Ti_5O_{12}$ nanosheets with a N-doped carbon coating for high rate lithium ion batteries, Adv. Funct. Mater. 23 (2013) 5429–5435.
[25] L. Shen, H. Li, E. Uchaker, X. Zhang, G. Cao, General strategy for designing core-shell nanostructured materials for high-power lithium ion batteries, Nano Lett. 12 (2012) 5673–5678.
[26] Y. Ma, B. Ding, G. Ji, J.Y. Lee, Carbon-encapsulated F-doped $Li_4Ti_5O_{12}$ as a high rate anode material for Li^+ batteries, ACS Nano 7 (2013) 10870–10878.
[27] J. Qiu, C. Lai, E. Gray, S. Li, S. Qiu, E. Strounina, C. Sun, H. Zhao, S. Zhang, Blue hydrogenated lithium titanate as a high-rate anode material for lithium-ion batteries, J. Mater. Chem. A 2 (2014) 6353–6358.
[28] Q. Guo, X. Cheng, Y. Shi, Z. Sheng, C. Chang, Bluish $Li_4Ti_5O_{12}$ with enhanced rate performance, J. Alloy. Comp. 710 (2017) 383–392.

[29] Q. Xia, N. Jabeen, S.V. Savitov, S.M. Aldoshin, H. Xia, Black mesoporous $Li_4Ti_5O_{12-d}$ nanowall arrays with improved rate performance as advanced 3D anodes for microbatteries, J. Mater. Chem. A 4 (2016) 17543–17551.
[30] H. Song, T.-G. Jeong, Y.H. Moon, H.-H. Chun, K.Y. Chung, H.S. Kim, B.W. Cho, Y.-T. Kim, Stabilization of oxygen-deficient structure for conducting $Li_4Ti_5O_{12-d}$ by molybdenum doping in a reducing atmosphere, Sci. Rep. 4 (2014) 4350.
[31] K.M. Colbow, J.R. Dahn, R.R. Haering, Structure and electrochemistry of the spinel oxides $LiTi_2O_4$ and $Li_{4/3}Ti_{5/3}O_4$, J. Power Souces 26 (1989) 397–402.
[32] D.C. Johnston, Superconducting and normal state properties of $Li_{1+x}Ti_{2-x}O_4$ spinel compounds. I. Preparation, crystallography, superconducting properties, electrical resistivity, dielectric behavior, and magnetic susceptibility, J. Low Temp. Phys. 25 (1976) 145–175.
[33] C.H. Chen, J.T. Vaughey, A.N. Jansen, D.W. Dees, A.J. Kahaian, T. Goacher, M. M. Thackeray, Studies of Mg-substituted $Li_{4-2x}Mg_xTi_5O_{12}$ spinel electrodes ($0 \leq x \leq 1$) for lithium batteries, J. Electrochem. Soc. 148 (2001) A102–A104.